Research Article | Vol. 8, No. 9 | 1 Sep 2017 | BIOMEDICAL OPTICS EXPRESS 4026
Biomedical Optics EXPRESS

Visible continuum pulses based on enhanced dispersive wave generation for endogenous fluorescence imaging

QUAN CUI,[1,2] ZHONGYUN CHEN,[1,2] QIAN LIU,[1,2] ZHIHONG ZHANG,[1,2] QINGMING LUO,[1,2] AND LING FU[1,2,*]

[1]*Collaborative Innovation Center for Biomedical Engineering, Wuhan National Laboratory for Optoelectronics-Huazhong University of Science and Technology, Wuhan, Hubei 430074, China*
[2]*Britton Chance Center and MOE Key Laboratory for Biomedical Photonics, School of Engineering Sciences, Huazhong University of Science and Technology, Wuhan, Hubei 430074, China*
[*]*lfu@mail.hust.edu.cn*

Abstract: In this study, we demonstrate endogenous fluorescence imaging using visible continuum pulses based on 100-fs Ti:sapphire oscillator and a nonlinear photonic crystal fiber. Broadband (500-700 nm) and high-power (150 mW) continuum pulses are generated through enhanced dispersive wave generation by pumping femtosecond pulses at the anomalous dispersion region near zero-dispersion wavelength of high-nonlinear photonic crystal fibers. We also minimize the continuum pulse width by determining the proper fiber length. The visible-wavelength two-photon microscopy produces NADH and tryptophan images of mice tissues simultaneously. Our 500-700 nm continuum pulses support extending nonlinear microscopy to visible wavelength range that is inaccessible to 100-fs Ti:sapphire oscillators and other applications requiring visible laser pulses.

OCIS codes: (180.4315) Nonlinear microscopy; (180.2520) Fluorescence microscopy; (060.4370) Nonlinear optics, fibers.

References and links

1. C. Li, R. K. Pastila, C. Pitsillides, J. M. Runnels, M. Puoris'haag, D. Côté, and C. P. Lin, "Imaging leukocyte trafficking in vivo with two-photon-excited endogenous tryptophan fluorescence," Opt. Express **18**(2), 988–999 (2010).
2. P. So, H. Kim, and I. Kochevar, "Two-Photon deep tissue ex vivo imaging of mouse dermal and subcutaneous structures," Opt. Express **3**(9), 339–350 (1998).
3. T. B. Krasieva, J. Ehren, T. O'Sullivan, B. J. Tromberg, and P. Maher, "Cell and brain tissue imaging of the flavonoid fisetin using label-free two-photon microscopy," Neurochem. Int. **89**, 243–248 (2015).
4. B. Kim, S. H. Lee, C. J. Yoon, Y. S. Gho, G.-O. Ahn, and K. H. Kim, "In vivo visualization of skin inflammation by optical coherence tomography and two-photon microscopy," Biomed. Opt. Express **6**(7), 2512–2521 (2015).
5. R. A. Xu, X. Q. Zhu, N. He, S. M. Zhuo, J. Xu, S. H. Jiang, H. S. Li, and J. X. Chen, "Multiphoton microscopic imaging of mouse intestinal mucosa based on two-photon excited fluorescence and second harmonic generation," J. Innov. Opt. Health Sci. **6**(01), 1350004 (2013).
6. W. Denk, "Two-photon excitation in functional biological imaging," J. Biomed. Opt. **1**(3), 296–304 (1996).
7. C. Xu, W. Zipfel, J. B. Shear, R. M. Williams, and W. W. Webb, "Multiphoton fluorescence excitation: new spectral windows for biological nonlinear microscopy," Proc. Natl. Acad. Sci. U.S.A. **93**(20), 10763–10768 (1996).
8. W. Denk, J. H. Strickler, and W. W. Webb, "Two-photon laser scanning fluorescence microscopy," Science **248**(4951), 73–76 (1990).
9. M. Yamanaka, K. Saito, N. I. Smith, Y. Arai, K. Uegaki, Y. Yonemaru, K. Mochizuki, S. Kawata, T. Nagai, and K. Fujita, "Visible-wavelength two-photon excitation microscopy for fluorescent protein imaging," J. Biomed. Opt. **20**(10), 101202 (2015).
10. J. Trägårdh, G. Robb, R. Amor, W. B. Amos, J. Dempster, and G. McConnell, "Exploration of the two-photon excitation spectrum of fluorescent dyes at wavelengths below the range of the Ti:Sapphire laser," J. Microsc. **259**(3), 210–218 (2015).
11. B. Sahoo, J. Balaji, S. Nag, S. K. Kaushalya, and S. Maiti, "Protein aggregation probed by two-photon fluorescence correlation spectroscopy of native tryptophan," J. Chem. Phys. **129**(7), 075103 (2008).

#297562 https://doi.org/10.1364/BOE.8.004026
Journal © 2017 Received 8 Jun 2017; revised 31 Jul 2017; accepted 31 Jul 2017; published 7 Aug 2017

Biomedical Optics EXPRESS

12. C. Li, C. Pitsillides, J. M. Runnels, D. Côté, and C. P. Lin, "Multiphoton Microscopy of Live Tissues With Ultraviolet Autofluorescence," IEEE J. Sel. Top. Quantum Electron. **16**(3), 516–523 (2010).
13. C. Li, R. K. Pastila, and C. P. Lin, "Label-free imaging immune cells and collagen in atherosclerosis with two-photon and second harmonic generation microscopy," J. Innov. Opt. Health Sci. **09**(01), 1640003 (2016).
14. W. Tao, H. Bao, and M. Gu, "Enhanced two-channel nonlinear imaging by a highly polarized supercontinuum light source generated from a nonlinear photonic crystal fiber with two zero-dispersion wavelengths," J. Biomed. Opt. **16**(5), 056010 (2011).
15. H. Tu, Y. Zhao, Y. Liu, Y. Z. Liu, and S. Boppart, "Noise characterization of broadband fiber Cherenkov radiation as a visible-wavelength source for optical coherence tomography and two-photon fluorescence microscopy," Opt. Express **22**(17), 20138–20143 (2014).
16. M.-C. Chan, C.-H. Lien, J.-Y. Lu, and B.-H. Lyu, "High power NIR fiber-optic femtosecond Cherenkov radiation and its application on nonlinear light microscopy," Opt. Express **22**(8), 9498–9507 (2014).
17. J. He, N. Wang, and T. Kobayashi, "Generation of stable two-color laser pulses in photonic crystal fiber for microscopy," Jpn. J. Appl. Phys. **53**(9), 092704 (2014).
18. H. Tu and S. A. Boppart, "Coherent fiber supercontinuum for biophotonics," Laser Photonics Rev. **7**(5), 628–645 (2013).
19. B. Yan, J. Yuan, X. Sang, K. Wang, and C. Yu, "Visible blue-shifted dispersive wave generation in the second-order mode of photonic crystal fiber," Opt. Eng. **55**(4), 046111 (2016).
20. X. Liang and L. Fu, "Enhanced Self-Phase Modulation Enables a 700–900 nm Linear Compressible Continuum for Multicolor Two-Photon Microscopy," IEEE J. Sel. Top. Quantum Electron. **20**(2), 42–49 (2014).
21. J. Palero, V. Boer, J. Vijverberg, H. Gerritsen, and H. J. C. M. Sterenborg, "Short-wavelength two-photon excitation fluorescence microscopy of tryptophan with a photonic crystal fiber based light source," Opt. Express **13**(14), 5363–5368 (2005).
22. X. Liu, A. S. Svane, J. Lægsgaard, H. Tu, S. A. Boppart, and D. Turchinovich, "Progress in Cherenkov femtosecond fiber lasers," J. Phys. D Appl. Phys. **49**(2), 023001 (2016).
23. J. M. Dudley, G. Genty, and S. Coen, "Supercontinuum generation in photonic crystal fiber," Rev. Mod. Phys. **78**(4), 1135–1184 (2006).
24. W. Wang, H. Yang, P. Tang, and F. Han, "Soliton trapping of dispersive waves during supercontinuum generation in photonic crystal fiber," Acta Phys. Sin-Ch. Ed. 62, 116–121 (2013).
25. G. P. Agrawal, *Nonlinear Fiber Optics* (Academic Press, 1995).
26. N. Akhmediev and M. Karlsson, "Cherenkov radiation emitted by solitons in optical fibers," Phys. Rev. A **51**(3), 2602–2607 (1995).
27. G. Genty, S. Coen, and J. M. Dudley, "Fiber supercontinuum sources (Invited)," J. Opt. Soc. Am. B **24**(8), 1771–1785 (2007).
28. G. P. Agrawal, "Nonlinear fiber optics: its history and recent progress [Invited]," J. Opt. Soc. Am. B **28**(12), A1–A10 (2011).
29. T. Sloanes, K. McEwan, B. Lowans, and L. Michaille, "Optimisation of high average power optical parametric generation using a photonic crystal fiber," Opt. Express **16**(24), 19724–19733 (2008).
30. N. Nishizawa and T. Goto, "Characteristics of pulse trapping by ultrashort soliton pulse in optical fibers across zerodispersion wavelength," Opt. Express **10**(21), 1151–1160 (2002).
31. L. Abrardi, S. Martin-Lopez, A. Carrasco-Sanz, F. Rodriguez-Barrios, P. Corredera, M. L. Hernanz, and M. Gonzalez-Herraez, "Experimental Study on the Role of Chromatic Dispersion in Continuous-Wave Supercontinuum Generation," J. Lightwave Technol. **27**(4), 426–435 (2009).

1. Introduction

Endogenous fluorophores, widely distributed in bio-tissue, are extensively used in bio-research to study their structure, functions and dynamics cellular energy metabolism [1–5]. In order to achieve biological imaging of endogenous fluorophores, two-photon microscopy, benefiting from its deep penetration, inherent sectioning ability, low photo-toxicity and noninvasive features, became the major optical imaging modality [6–8]. For ultraviolet (UV) endogenous fluorophores, such as tryptophan, melanin and the reduced form of nicotinamide adenine dinucleotide (NADH), the two-photon excitation spectrum is located in the visible range [9, 10]. It has been reported that the optimal two-photon excitation wavelengths for NADH are about 700 nm, while 500-580 nm for tryptophan. Therefore, it is impossible to provide efficient two-photon excitation of multiple UV endogenous fluorophores using near infrared (NIR) wavelength pulses from a 100-fs Ti:sapphire oscillator, which is a standard light source. Thus, visible ultrashort pulse is essential for endogenous fluorescence imaging to provide information about complex biological phenomena without exogenous labels.

There are two approaches to produce visible ultrashort pulse. The first one is to employ optical parametric oscillator (OPO) system combined with 100-fs Ti:sapphire oscillator to generate visible pulses through second harmonic generation (SHG). OPO system has been

Biomedical Optics EXPRESS

used for two-photon microscopy of both UV excitable fluorescent dyes and endogenous fluorophores [11–13]. However, bulky OPO systems never offer low-cost or simple solutions. The slow tuning process and narrow spectral bandwidth also limit its applications. The other is dispersive wave (DW) generation, which is a promising choice for generating visible laser pulses because it offers the benefits of simplicity and large tunability region. DW generation, as a fiber nonlinear effect, originates from the perturbation of a stable temporal soliton by higher-order fiber dispersion [14–16]. The process of SC generation is mainly dominated by soliton effect when ultrafast pump pulse lies in the anomalous dispersion of fiber. Then high order soliton breaks into its fundamental components through fission process and each individual soliton component emits DW pulses. Phase-matching condition between the solitons and DW pulses determines the specific wavelength of emitted DW pulses. A general study based on the phase matching condition shows that the positive third order dispersion always generates a blue peak as DW pulses, which falls below the pumping wavelength. Thus, the control of dispersion and the nonlinearity properties offered by a photonic crystal fiber (PCF) enables continuum generation to convert the energy of NIR laser, through DW generation, to visible even ultraviolet spectral regions [17–19]. However, there were only few reports on performing two-photon imaging using fiber-based DW pulse in the visible wavelength range [20].

The application of current visible continuum pulses based on DW generation is limited for several reasons. First, visible DW pulses, on the order of 1 mW, are much smaller than those required for tissue imaging. Second, the spectral bandwidth of DW pulses is limited to tens of nanometers, which is too narrow to cover peak excitation wavelengths of multiple fluorophores. Third, fiber dispersion and nonlinear effects seriously stretch femtosecond pulses to picosecond durations, which leads to reduced two-photon excitation and low-level fluorescence signals. Yet, there is no such visible continuum pulse with broadband spectrum and high average power demonstrated for nonlinear imaging.

In this paper, visible continuum pulses and its application to endogenous fluorescence imaging were both reported. Broadband (500–700 nm) and high-power (150 mW) continuum pulses are generated based on enhanced dispersive wave generation by pumping 100-fs Ti:sapphire femtosecond pulses into the anomalous dispersion region near the zero-dispersion wavelength (ZDW). We also minimize the continuum pulse width by determining the proper fiber length, which is long enough to provide efficient generation of visible continuum pulses while the dispersion-induced pulse broadening effect is at a minimum. We demonstrate two-photon microscopy using visible continuum pulses and obtain NADH and tryptophan images of mice tissues at the same location simultaneously. The continuum pulses could extend nonlinear microscopy to visible wavelength region that currently is inaccessible to 100-fs Ti:sapphire oscillators.

2. Experimental setup

Figure 1 presents the system configuration of the custom-built two-photon microscope system with visible continuum generation. The continuum-generation system used a commercially available femtosecond Ti:sapphire oscillator (Spectra-Physics Mai Tai BB, Newport Corporation, Irvine, California) as the pump source. A PCF (NL-2.2-830, NKT Photonics, Birkerød, Denmark) was used as a wavelength down-convertor because of its high nonlinear coefficient of 70 $W^{-1}\cdot km^{-1}$. The dispersion properties of the NL-830 PCF are depicted in the inset of Fig. 1. An optical isolator, noted here as the Faraday isolator, was inserted after the Ti:sapphire femtosecond laser to avoid backward reflection from the PCF into the laser cavity that could destroy the laser's mode locking. A pair of gratings compensated for the group velocity diversion (GVD) introduced by the optical isolator and coupled objectives to ensure that the pump pulse width was minimized. The spectral analysis of the visible continuum pulse was conducted with a spectrometer (USB2000 + , Ocean Optics, Inc., Dunedin, Florida). A short-pass filter, placed after the second collimating objective, blocked the light

Biomedical Optics EXPRESS

above 700 nm and enabled the characterization of visible continuum pulses. The setup used a milliwatt power meter (PD300-3W, Ophir Corporation, Jerusalem, Israel) to measure the power of the continuum pulses.

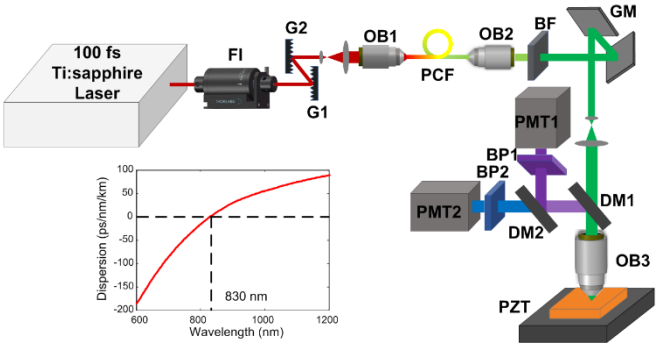

Fig. 1. Experimental setup for visible-wavelength two-photon microscopy using a fiber continuum based on enhanced dispersive wave generation. FI: Faraday isolator; I G: grating; OB: objective; GM: galvomirror; BF: block filter; BP: band-pass filter; DM: dichroic mirror; and PMT: photomultiplier tube. The inset illustrates the dispersion properties of NL-830 PCF.

The microscope system is composed of a galvanometer-based x–y optical scanner (6215H, Cambridge Technology, Inc., Bedford, Massachusetts) and a fixed-stage upright microscope (BX51WI, Olympus Corporation, Tokyo, Japan). All optics in the custom-built microscope system were selected to allow the transmission of 500 nm to 700 nm visible light. A water-immersion microscope objective (25 × , NA 1.05 UPlan, Olympus America Inc., Center Valley, Pennsylvania) was used to focus on the sample and collect fluorescence signals. A piezoelectric stage (P-563.3CD, Physik Instrumente, Karsruhe, Germany) was used for z scanning. In order to demonstrate the feasibility of the method using fiber continuum pulses to achieve visible-wavelength two-photon microscopy, we choose endogenous fluorophores NADH and tryptophan for this research. Their two-photon-excited fluorescence signal was detected using two photomultiplier tubes, PMT1 and PMT2 (H7422A-40, Hamamatsu Photonics K.K., Hamamatsu City, Japan). Green and red channels were created by placing band-pass filters BP1 (FF02-377/50-25, Semrock, Inc., Lake Forest, Illinois) and BP2 (FF01-445/45-25, Semrock, Inc., Lake Forest, Illinois) in front of the two PMTs.

3. Experimental characterization of the visible continuum pulses

3.1 Numerical and experimental evaluation of DW generation

Multiple fiber nonlinear effects have been adopted to generate continuum pulses. However, for the reported common nonlinear effects such as self-phase modulation (SPM), and four wave mixing (FWM), the peak power of the pump pulses rapidly decreases because of high normal dispersion. This decrease limits the spectral broadening to only dozens of nanometers so that no visible components can be obtained with infrared pump pulses [21]. Soliton effect serves as down-frequency convertor which would also be difficult to produce visible spectral components.

Among the various nonlinear processes, the generation of blue spectral components through DW generation has received considerable attention for its broad-range tunability, low noise, compactness, durability, and ease of service-free operation. DW generation originates from the perturbation of a stable temporal soliton by higher-order fiber dispersion [22–24]. When solitons propagate in anomalous dispersion region with positive third-order dispersion, the DW pulses are emitted at a shorter wavelength than that of the solitons. Wavelength shifting of hundreds of nanometers can be achieved by DW generation. Thus, the DW generation can be used to convert the near-infrared pump pulses to visible-wavelength or

Biomedical Optics EXPRESS

even shorter-wavelength spectral components. The location of the DW pulse is determined by the phase-matching condition referring to the dispersion and nonlinear contribution [25],

$$\sum_{n\geq 2}\frac{\left(\omega_{DW}-\omega_{p}\right)^{n}}{n!}\beta_{n}\left(\omega_{p}\right)=\frac{\gamma P_{p}}{2}, \tag{1}$$

where ω_{DW} and ω_{p} are the central frequencies of the DW and pump pulses. Here, γ and Pp are the nonlinear coefficients of the fiber and peak power of the pump pulses, respectively. βn represents the nth derivative of the dispersion coefficient taken at ω_{p}.

So, we considered pumping at the anomalous dispersion region and using DW generation as a wavelength down-convertor to achieve a visible laser source. With the dispersion of NL-830 PCF, the central wavelength of the DW pulse at different pump powers and wavelengths is numerically solved by Eq. (1), as shown in Fig. 2. The simulation shows that the central wavelength of DW decreases monotonically with increases in pump power. In addition, the central wavelength of DW shifts toward shorter wavelengths as the pump wavelength shifts toward longer wavelengths. These simulation results provide theoretical guidance for the following experiment.

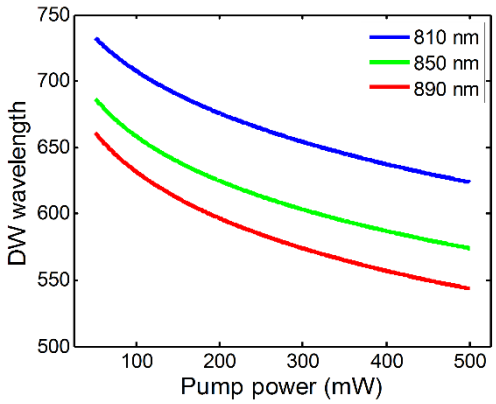

Fig. 2. Simulated phase-matching conditions between DW and pump wavelengths with different pump powers according to Eq. (1).

This experiment investigated nonlinear effects using different pump wavelengths by pumping 100 fs femtosecond-laser pulses through a 6 cm PCF. Guided by the numerical calculation shown in Fig. 2, we tuned the pump pulse at 890 nm in the anomalous dispersion region to generate visible continuum pulses through the DW generation. Figure 3 shows the output continuum spectra. With a relatively low pump power of 100 mW, the DW pulse had already arisen because the pump pulses located in the high anomalous dispersion region formed a high-order soliton, emitting DW pulses in the normal dispersion region. As the pump power increased from 100 mW to 500 mW, the visible part of the output continuum was located at visible wavelengths of 550 nm to 650 nm through the DW generation. This result agrees well with the simulation results shown in Fig. 2.

Biomedical Optics EXPRESS

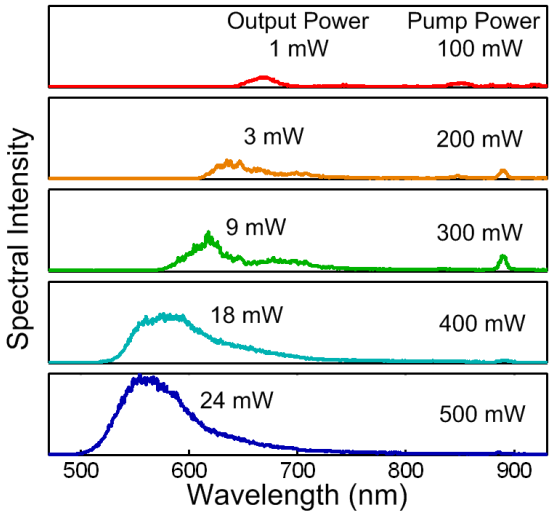

Fig. 3. Continuum generation using a 6 cm PCF, having a pump wavelength of 890 nm, in the high anomalous dispersion region. The output power of the visible continuum pulses increases as the pump power increases from 100 mW to 500 mW.

Here, we considered that the DW pulses contributed most of the power distributed below 700 nm as predicted by the numerical simulation. DW conversion efficiency is defined as the ratio between the measured power of the DW pulse and the total PCF output power. When a coupling efficiency of 50% was achieved, the measures of the DW pulse output power were 1 mW, 3 mW, 9 mW, 18 mW, and 24 mW. The corresponding DW conversion efficiencies were 2%, 3%, 6%, 9%, and 10%, respectively. Generating visible continuum pulses through the DW generation is possible; however, the visible continuum pulses suffer from low output power. In addition, the spectral bandwidth of DW pulses is limited to dozens of nanometers and cannot be broadened further. In conclusion, visible continuum pulses generated through only DW generation by pumping in high-anomalous dispersion regions are not suitable for nonlinear microscopy because of their limited average power and narrow spectral bandwidth.

3.2 Enhanced DW generation for visible continuum pulses

Since the obtained visible continuum pulses suffered from limited average power and narrow spectral bandwidth, the DW generation should be enhanced. It is known that the DW radiation is emitted only when the soliton spectrum overlaps with the DW generation. The amplitude of the DW radiation is proportional to the amplitude of the soliton at the phase-matched frequencies [26]. From the simulation of Eq. (1), to generate blue shifted DW pulses, the pump wavelength should be tuned away from ZDW in the anomalous region. However, the gap between the pump and DW pulses increases at the same time. For this reason, the pump wavelength should be further optimized in order to allow for a reasonable overlap between DW and pump pulse at the normal dispersion region to be obtained.

Pump wavelength, which determines fiber-introduced dispersion, plays a governing role in controlling the type of nonlinear effects participating in continuum generation. According to the earlier reports, in contrast with pumping at high-normal or anomalous dispersion regions, when an ultrashort optical pulse is located near the ZDW of the PCF, unusual continuum generation is expected [27–29]. Since the broadened pulse spectrum experiences opposite types of dispersion across the ZDW point, multiple nonlinear effects contribute to spectral overlap between DW and pump pulse. Therefore, aiming at generating high power and broadband visible continuum pulses, pumping near the ZDW of the PCF could enhance DW generation. We investigated the continuum generation process with pump wavelengths of

Biomedical Optics EXPRESS

810 nm and 850 nm, at which pump pulses experienced low-positive and low-negative dispersions, respectively.

We tuned the pump pulse at 810 nm near the ZDW in normal dispersion region to generate visible continuum pulses through multiple nonlinear effects. The output continuum spectra, shown in Fig. 4, manifested significant differences from the corresponding continuum spectra resulting from pumping at 890 nm. At the initial stage, when the pump power was 100 mW and 200 mW, the pulse broadened mainly by SPM arising from normal dispersion. Because the pump wavelength was located close to the ZDW of the PCF, the FWM occurred and generated anti-Stokes sidebands at wavelengths of 750 nm, 740 nm, and 730 nm, corresponding to pump powers of 300 mW, 400 mW, and 500 mW, respectively. When the pump power exceeded 300 mW, small peaks appeared in the visible wavelength regions. This result occurred because the pump energy was extended to the anomalous dispersion region of the PCF. Then, the soliton was formed and emitted DW pulses at wavelengths of 650 nm, 625 nm, and 610 nm, respectively, matching the simulation results shown in Fig. 2.

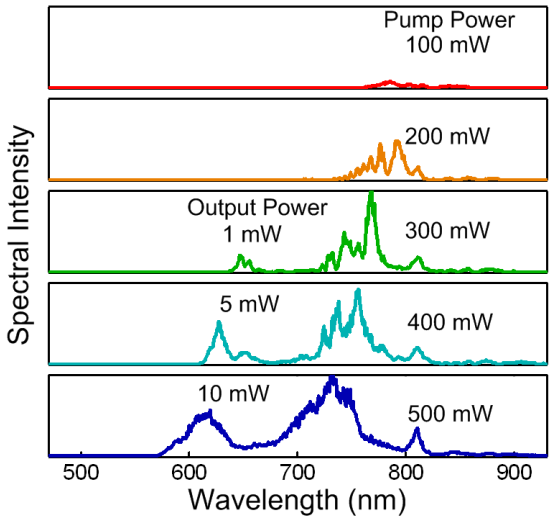

Fig. 4. Continuum generation using a 6 cm PCF with a pump wavelength of 810 nm, located at the low normal dispersion region near the ZDW. The output power of the visible continuum pulses increases as the pump power increases from 300 mW to 500 mW.

Even though a broadband continuum with a spectrum from 600 nm to 800 nm was achieved through the combined nonlinear effects of FWM and DW, the output power of the generated visible continuum pulse, less than 10 mW, was weak. This is because that only a small part of the pump pulse extended into the anomalous dispersion region through SPM. Therefore, the soliton effect was weak and the corresponding visible DW conversion efficiency, measured below 5%, was not efficient. Thus, the visible continuum pulse generated by pumping at the normal dispersion region near the ZDW is not suitable for nonlinear microscopy.

In order to keep the DW generation the major role during continuum generation, the pump wavelength was tuned to 850 nm near ZDW in the anomalous dispersion region. Blue-shifted DW pulses were generated from 680 nm to 560 nm, as shown in Fig. 5, agreeing well with the simulation results shown in Fig. 2. Because pump wavelength was near ZDW, the generated continuum pulse was much broadened by SPM and FWM. The anti-Stokes sidelobes at wavelengths of 750 nm, 720 nm, and 700 nm, corresponding to pump powers of 300 mW, 400 mW, and 500 mW, were generated through FWM. As the pump power

Biomedical Optics EXPRESS

exceeded 300 mW, the DW pulse mixed with SPM and FWM pulses to form broadband and flat visible continuum pulses, measured to be 60 mW, 108 mW, and 150 mW. As the pump power increases to 500 mW, visible broadband (500-700 nm) continuum pulses were achieved.

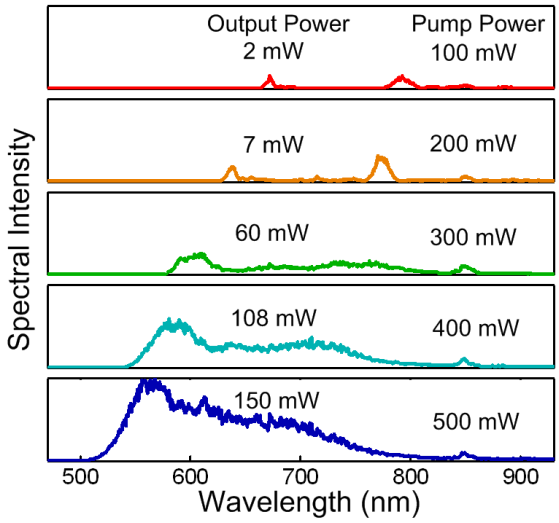

Fig. 5. Continuum generation using a 6 cm PCF with a pump wavelength of 850 nm, located at a low anomalous dispersion region near the ZDW. The output power of the visible continuum pulses increased as the pump power increased from 100 mW to 500 mW.

It is worth noting that, at the same input power, the DW conversion efficiency was much higher with 850 nm pump pulses than with 890 nm pump pulses. This phenomenon can be explained using two mechanisms. First, note that the dispersive wave generation is effectively amplified with the overlap between the spectrum of the pump and that of the DW is large enough. When the pump wavelength is located near the ZDW, the continuum spectrum is much broadened because of SPM and FWM, providing enough spectral overlap. Second, pulse trapping effect would further enhance DW generation in the normal dispersion region. Pulse trapping is defined as an optical signal pulse in the normal dispersion region trapped by a soliton pulse in the anomalous dispersion region [30]. When these two pulses propagate along the fiber, the trapped pulse in the normal dispersion region shifts to the shorter wavelength while the soliton pulse shifts to the longer wavelength. The soliton pulse is perturbed by the cross-phase modulation from the trapped signal pulse, which leads to the soliton pulse transferring part of its energy to the trapped pulse [31]. As the spectral components from SPM and FWM extend into the normal dispersion region, working as trapped signal pulse, sufficient spectral components are shared by the soliton and the DW. Thus, more energy transfers from the soliton to the visible spectra through pulse trapping. In conclusion, the enhanced dispersive wave generation by pumping near the ZDW of the PCF with anomalous dispersion support the generation of high-power and broadband continuum pulses in the visible range.

3.3 Fiber length dependence on ultrashort pulses

In addition to pump wavelength, fiber length is also a key factor influencing continuum generation. A longer PCF can generate a fiber-optic continuum source with higher DW conversion efficiency. However, fiber length also is related to the temporal pulse width of output pulses. Because the demonstrated visible continuum source always is located in the normal dispersion region, it experiences severe pulse broadening when propagating through

Biomedical Optics EXPRESS

the PCF. In nonlinear microscopy, the broadening femtosecond pulse leads to degradation of fluorescence signals. Therefore, it is important to find a proper fiber length, which induces the minimum dispersion while the DW conversion efficiency is strong.

The output spectra in the visible region were generated by pumping 100 fs, 500 mW pulses through PCFs of 2 cm, 4 cm, 6 cm, 15 cm, and 30 cm, as Fig. 6 shows, to determine the proper fiber length. At short fiber lengths from 2 cm to 6 cm, DW conversion efficiency increased from 10% to 20%. However, for the 6 cm, 15 cm, and 30 cm PCFs, similar output continuum pulses in the visible region were obtained. The DW conversion efficiency remained the same. These results occurred because the continuum generation process tends to saturate when the pump pulse is stretched and because peak power decreases for propagation lengths exceeding 6 cm. We used visible continuum pulses to achieve TPEF imaging of tryptophan powder ($C_{11}H_{12}N_2O_2$, Sigma, Germany) and to characterize the pulse-width of the generated pulses because the two-photon fluorescence signal is inversely proportional to related pulse widths. Results appear in Fig. 6.

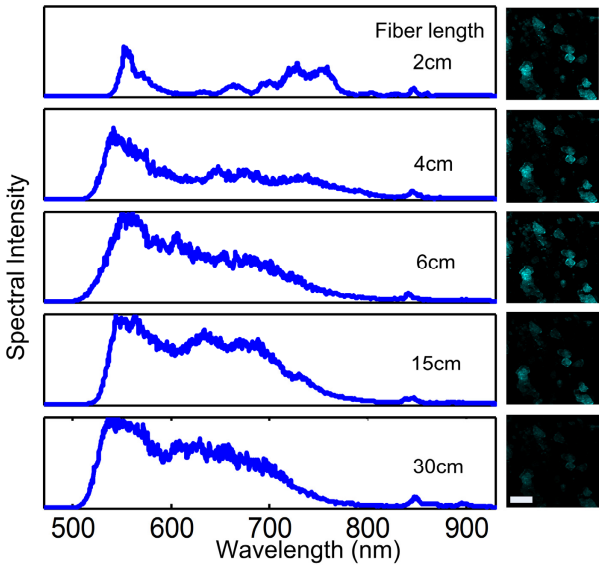

Fig. 6. Continuum spectra at the ends of the 2 cm, 4 cm, 6 cm, 15 cm, and 30 cm PCFs and the corresponding two-photon fluorescence images of tryptophan powder. All two-photon fluorescence images were acquired using visible continuum pulses with the same power and spectra. Decreasing fluorescence signals result from broadened pulse widths. Scale bar: 20 μm.

All two-photon fluorescence images were acquired using same excitation power (2 mW); the same spectral components were sliced by an optical filter (FF01-550/17-25, Semrock, Inc., Lake Forest, Illinois). When the lengths of the PCF were 2 cm, 4 cm, and 6 cm, the fluorescence signal remained constant. For tested propagation lengths exceeding 6 cm, namely, 15 cm and 30 cm, the signal decreased as the propagation increased. This result indicates that the continuum pulses mainly experienced pulse-broadening effects after encountering the first 6 cm of fiber. Thus, the broadened temporal pulse width led to reduced two-photon fluorescence signals. When the fiber length was 6 cm, a high-power visible continuum pulse was generated, and the pulse-broadening effects were minimized, thus enhancing the excitation efficiencies of the nonlinear signals. Therefore, the results of this experiment support the conclusion that the optimum PCF length for nonlinear microscopy is 6 cm.

Biomedical Optics EXPRESS

4. Endogenous fluorescence imaging using visible continuum pulses

We achieve endogenous fluorescence imaging using visible continuum pulses as light source. Skin and kidney tissues from mice were adopted as the subjects for imaging of NADH and tryptophan fluorescence. C57BL/6 mice weighing ~20 g was purchased from the Zhongnan Hospital of Wuhan University (Hubei, China). The C57BL/6 mice were anaesthetized by intraperitoneal injection of urethane (90 μL/10 g) then dissected to extract ear skin and kidney. All experiments were performed according to the animal experiment guidelines of the Animal Experimentation Ethics Committee of Huazhong University of Science and Technology (Hubei, China).

The optimal two-photon excitations for NADH and tryptophan are in visible range about 700 nm and 560 nm, respectively, which are not in the wavelength range of traditional lock-on Ti:sapphire lasers. The emission of tryptophan occurs around 350 nm, which is lower than the 450 nm wavelength commonly used for NADH tissue imaging. The detection channel for NADH used in this experiment spanned 422 nm to 467 nm. Because endogenous fluorophores have broad emission spectra, the detected NADH signal could show contributions from other fluorophores. The detection channel for tryptophan spans 352 nm to 402 nm; in this range, endogenous fluorescence is dominated by tryptophan signals. The dependence of fluorescence intensity on excitation power was measured. The resulting quadratic dependence indicated two-photon excitation. As discussed above, this demonstration used a 6 cm wavelength-conversion PCF as the visible laser source. The setup employed pump power of 500 mW; the output of the continuum pulses between 500 nm and 700 nm, covering the two-photon absorption spectra of NADH and tryptophan, was connected directly to the custom-built microscope.

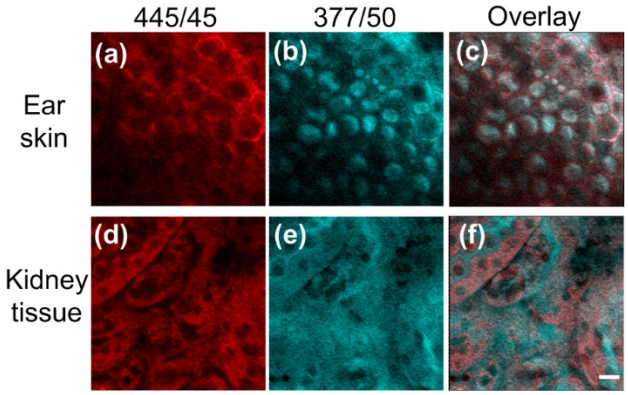

Fig. 7. Two-photon imaging of mice tissues using visible continuum pulses. NADH fluorescence image (a) and tryptophan fluorescence image (b) of ear skin at a depth of about 30 μm. (c) Overlay of (a) and (b). NADH fluorescence image (d) and tryptophan fluorescence image (e) of kidney tissue. (f) Overlay of (d) and (e). Scale bar: 20 μm.

Two-photon images of mice ear skin and kidney tissue were obtained using the 500-700 nm continuum pulses. Figures 7(a) and 7(b) show NADH and tryptophan fluorescence images of mice ear skin; depicted is the dermis layer at a depth of approximately 30 μm. Figure 7(b) illustrates the shape of the dermal cells; the nuclei appear darker than the cytoplasm because the UV fluorescence signals come primarily from tryptophan rather than from the nuclei. The NADH and tryptophan fluorescence images of mice kidney tissue in Figs. 7(d) and 7(e) show features of the proximal tubule segments. The fluorescence intensity in Fig. 7(e) shows much more even distribution than in Fig. 7(d) because the UV fluorescence signal comes primarily from the protein components of the cytoplasm while the NADH fluorescence signal has a punctuated pattern. These square images are 256 × 256 pixels and present fields of view of 150 × 150 μm. Exposure time of each pixel is 16 μs. Excitation power at the sample was

Biomedical Optics EXPRESS

approximately 20 mW. Based on the galvamirror in our system, the minimum pixel exposure time we used is 4 μs, which is adequate for two-photon tissue imaging. With excitation power between 20 mW and 30 mW, the autofluorescence are efficiently excited and no photobleaching or phototoxicity occurred within 30 s. The image performance based on our visible continuum pulses is comparable to instances of SHG obtainable from commercially available OPOs [13]. The continuum generation technique based on enhanced dispersive wave generation provides an important laser source suitable for nonlinear microscopy in the visible wavelength region.

5. Conclusion

In summary, we demonstrated visible continuum pulses generation technique and its application to endogenous fluorescence imaging. High-power and broadband continuum pulses in the visible wavelength region were achieved using the enhanced dispersive wave generation when pumping pulses near the ZDW of the PCF with anomalous dispersion using conventional 100-fs Ti:sapphire oscillator. We also determined the proper fiber length for efficient visible continuum generation while minimizing the dispersion-induced pulse-broadening effect. Visible-wavelength two-photon endogenous fluorescence imaging offers the potential for supporting the analysis of certain molecules in tissue structures. Visible continuum pulses generation, benefiting from simple system configuration, convenient wavelength conversions and broad spectra encompassing the 500–700 nm region, is suitable for nonlinear microscopy. Thus, it could see wide use in fundamental biomedical research and future clinical applications.

Funding

National Natural Science Foundation of China (61522502); Science Fund for Creative Research Group of China (61421064); The Director Fund of WNLO.

Acknowledgments

We thank Jiafu Wang and Hua Li for providing the mice tissue samples. We thank Ying Wang for many helpful discussions.

Disclosures

The authors declare that there are no conflicts of interest related to this article.